


Article

Research on Panel Flutter Considering the Effect of Convective Active Cooling

Jie Huang ^{1,2} , Weishuang Lu ¹, Guowei Yang ^{1,2} and Guannan Zheng ^{1,3,*}

¹ Key Laboratory for Mechanics in Fluid Solid Coupling Systems, Institute of Mechanics, Chinese Academy of Sciences, Beijing 100190, China; huangjie@imech.ac.cn (J.H.)

² School of Engineering Science, University of Chinese Academy of Sciences, Beijing 100191, China

³ School of Future Technology, University of Chinese Academy of Sciences, Beijing 100191, China

* Correspondence: zhengguannan@imech.ac.cn

Abstract: The aeroelastic characteristics of the panel under the action of coolant are obviously different from the flutter characteristics of the traditional panel. In order to solve this problem, the dynamics model of the panel flutter was established in this paper based on von Karman's large deformation theory and the Kirchhoff–Love hypothesis. The panel dynamics equations were discretized into constant differential equations with finite degrees of freedom by Galerkin's method, and solved by the fourth Runge–Kutta method in the time domain. The nonlinear modified piston theory was used to predict the unsteady aerodynamic loads, and the accuracy of the flutter analysis model was verified. On this basis, the effects of the head-panel pressure of coolant, the pressure drop ratio, the coolant injection direction, and the inertial resistance and viscous resistance on panel stability and flight stability were investigated, respectively. The results showed that reducing the pressure drop ratio, and reducing or increasing the head-panel pressure (valuing away from the freestream pressure) can improve the critical dynamic pressure when bifurcation occurs. At $M_\infty = 5.0$, the pressure drop ratio causes a 22.1% increment in the critical dynamic pressure. The influence of the coolant injection direction on the panel bifurcation is mainly influenced by the head-panel pressure. The inertial resistance slows down the convergence process of the panel response, increases the limit cycle amplitude, and reduces the critical dynamic pressure of the panel, while the viscous resistance plays the opposite role. Based on these conclusions, this paper finally proposes the suppression method of panel fluttering from head-panel pressure, inertial resistance, viscous resistance, etc.

Keywords: panel flutter; coolant action; flight stability; flutter suppression



Citation: Huang, J.; Lu, W.; Yang, G.; Zheng, G. Research on Panel Flutter Considering the Effect of Convective Active Cooling. *Appl. Sci.* **2023**, *13*, 4925. <https://doi.org/10.3390/app13084925>

Academic Editor: Junhong Park

Received: 28 March 2023

Revised: 11 April 2023

Accepted: 13 April 2023

Published: 14 April 2023



Copyright: © 2023 by the authors. Licensee MDPI, Basel, Switzerland. This article is an open access article distributed under the terms and conditions of the Creative Commons Attribution (CC BY) license (<https://creativecommons.org/licenses/by/4.0/>).

1. Introduction

As the most basic structural unit of a vehicle, panels have the characteristics of a simple structure, easy loading and unloading, a high load-bearing capacity, etc. They are widely used in the key parts of the wing fuselage skin and air intakes of hypersonic vehicles. However, a dangerous dynamic instability phenomenon, panel flutter [1,2], often occurs in actual flight. This is a self-excited oscillation under the coupling of aerodynamic, elastic, and inertial forces, which has strong nonlinear characteristics. Under high dynamic pressure conditions, the structure is prone to Limit Cycle Oscillation (LCO) and dynamic instability, which reduces the fatigue life of the panel and even causes damage. For example, in the late 1950s, NASA's X-15 test aircraft experienced severe structural vibration in the tail and fairing panels on its first flight, and the conditions of occurrence were much lower than one atmosphere pressure [3]. Therefore, the study of panel flutter is of great importance for flight safety and aircraft performance assessment.

The systematic study of panel flutter began in the 1950s [4,5]. Dowell [4] analyzed the panel flutter in supersonic airflow using Galerkin's method, in which the aerodynamic force prediction was based on linear piston theory. The results of the analysis revealed

the induced mechanism and evolutionary history of plate aeroelasticity, and gave the critical dynamic pressure of flutter. It was also pointed out that at least sixth-order modes were required to obtain a more accurate solution. These constructive results provided an important reference for the subsequent research on panel flutter problems. Xue et al. [6] presented a frequency domain method for two-dimensional nonlinear panel flutter with thermal effects obtained from a consistent finite element formulation. The deformation was obtained by von Karman's nonlinear strain–displacement relation, and the quasi-steady first-order piston theory was employed for aerodynamic loading. The results presented the influence of temperature and dynamic pressure on panel fatigue life. Guo and Mei [7] investigated the thermo-aeroelastic vibration response of a panel using the structural modal method, which can drastically reduce the number of coupled nonlinear modal equations for the large amplitude nonlinear panel flutter analysis. Using the Ritz method to study the panel aeroelasticity problem, Song and Li [8] pointed out that the aerodynamic force can significantly change the modal vibration pattern of the structure. Focusing on the flutter problem of composite laminate, Koo et al. [9] and Singha et al. [10] established the panel flutter dynamics model based on the finite element method, and discussed the effect of structural and aerodynamic damping. The results indicated that the degree of influence of structural damping on the panel dynamic characteristics is affected by the aerodynamic damping and the fiber layup direction. The effect of structural damping is weak when the aerodynamic damping is large, while the opposite results are obtained when the aerodynamic damping is small. Hamid and Mohammad [11] presented the nonlinear vibrational frequency analysis of a curved panel under the effects of in-plane compressive and tensile loads, carried out for the first time in the time domain. The first- and third-order piston theories were incorporated for the nonlinear curved panel flutter analysis under the effects of in-plane and thermal loads. Cheng et al. [12] analyzed the dynamic response of panels in a hypersonic flight environment and pointed out that there are differences in the history of panels to reach chaotic motion at different flight Mach numbers. Xie et al. [13] considered both aerodynamic nonlinearity and structural nonlinearity in panel flutter analysis, in which third-order piston theory was used for nonlinear aerodynamic loading. The effects of each item of piston theory on panel flutter were studied. The results showed that the geometric term in the quadratic term is the main cause of nonlinearity. Culler et al. [14] developed a comprehensive aerothermoelastic model for the analysis of panel structures in hypersonic flow, and investigated the impact of fluid–thermal–structural coupling on aerothermoelastic behavior using Galerkin's method and the third-order piston theory. Chen et al. [15] analyzed the aeroelastic flutter of a composite panel with functionally graded material. The result illustrated that adding a few amounts of grapheme nanoplatelets can effectually enhance the aeroelastic properties of the plates. The displacement and acceleration feedback control are used to suppress the occurrence of the panel flutter.

During hypersonic flight, the outer surface wall structure of the vehicle is subjected to a rather harsh aerodynamic thermal environment, which seriously affects the performance and flight safety of the vehicle [16]. The convection cooling system is one of the most commonly used thermal protection strategies [17–20]. For instance, Castaldi [18] presented an effective endothermic fuel platform for regeneratively cooled hypersonic vehicles. The current research on the convection cooling thermal protection system mainly focuses on optimal control [21], thermal protection efficiency improvement [16,22], structure simplification, and mass reduction [23], but has not yet considered the influence of the coolant force on the stability of the wall plate. Therefore, the dynamics model of panel flutter under the action of coolant is established in this paper based on von Karman's large deformation theory and the Kirchhoff–Love hypothesis. The kinetic equations are discretized by Galerkin's method in the space domain and solved by the fourth Runge–Kutta method in the time domain. Based on this, the effects of the head-panel pressure of the coolant, the pressure drop ratio, the coolant injection direction, and the inertial resistance and viscous

resistance on panel stability and flight stability were investigated, respectively, and the suppression method of panel flutter was proposed.

This paper is organized as follows. Section 2 presents the dynamic analytical model of panel flutter under the effect of coolant and verifies the accuracy of the model. Section 3 analyzes the panel stability under the influence of coolant. Section 4 analyzes the flight stability of the panel and proposes the suppression method of panel flutter. The conclusions are summarized in Section 5.

2. Theoretical Analysis

Consider a two-dimensional isotropic simply-supported panel, as shown in Figure 1, where the panel length is a , the thickness is h , and the transverse vibration displacement is $w(x)$. The upper surface of the panel is acted on by supersonic airflow, and the Mach number, pressure, and density of the freestream are $Ma_\infty, p_\infty, \rho_\infty$, respectively. Below the panel is a convective cooling channel filled with coolant driven by a constant pressure gradient $-G$, ignoring the viscous shear. Based on von Karman’s large deformation thin plate theory and the Kirchhoff–Love hypothesis, the equation of motion for the panel is

$$\rho h \frac{\partial^2 w}{\partial t^2} + D \frac{\partial^4 w}{\partial x^4} - (N_x + N_0) \frac{\partial^2 w}{\partial x^2} + (p - p_\infty) = f_c - p_\infty \tag{1}$$

The boundary conditions are

$$\begin{cases} w(0, t) = w(1, t) = 0 \\ \frac{\partial^2 w}{\partial x^2}(0, t) = \frac{\partial^2 w}{\partial x^2}(1, t) = 0 \end{cases} \tag{2}$$

where w is transverse vibration displacement, ρ is material density, $D = Eh^3 / [12(1 - \nu^2)]$ is bending stiffness, E is elastic modulus, ν is Poisson’s ratio. N_0 is in-plane load caused by assembly or heating, and N_x is nonlinear membrane load caused by panel deformation.

$$N_x = \frac{Eh}{2a} \int_0^a \left(\frac{\partial w}{\partial x} \right)^2 dx \tag{3}$$

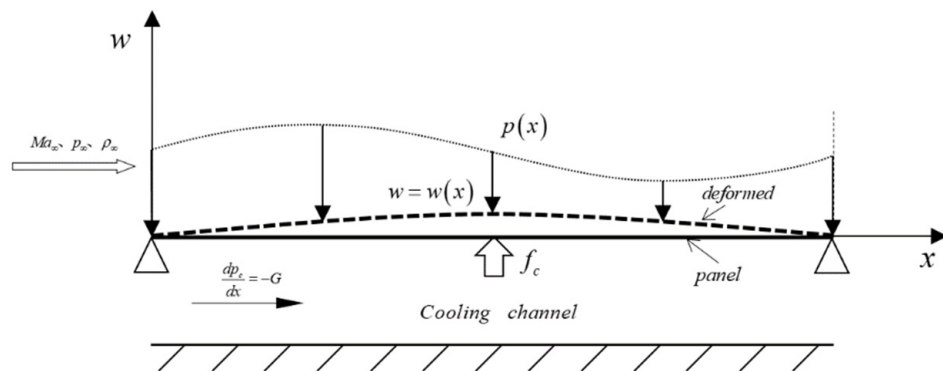


Figure 1. Geometric model of panel with cooling channel.

In order to predict the aerodynamic load under supersonic/hypersonic conditions accurately, the nonlinear modified piston theory [13] is used.

$$p - p_\infty = \frac{2q}{\sqrt{M_\infty^2 - 1}} \left[\frac{1}{U_\infty} \left(\frac{M_\infty^2 - 2}{M_\infty^2 - 1} \right) \frac{\partial w}{\partial t} + \frac{\partial w}{\partial x} + \frac{\gamma + 1}{4} M_\infty \left(\frac{\partial w}{\partial x} \right)^2 \right] \tag{4}$$

U_∞ is the velocity of freestream and $q = \rho_\infty U_\infty^2 / 2$ is dynamic pressure.

The coolant load on the panel is

$$f_c = p_c + f_{in} + f_{vis} \tag{5}$$

The three items on the right side of Equation (5) are coolant pressure, inertial resistance, and viscous resistance. The flow of the coolant in the cooling channel is approximated by the Poiseuille flow. It is called forward flow when the coolant and air flow are in the same direction; otherwise, it is the reverse flow. Take forward flow as an example

$$p_c = p_{ch} - Gx \tag{6}$$

p_{ch} is the head-panel pressure. The inertial resistance and viscous resistance are proportional to the second derivative and the first derivative of the deformation to time, respectively.

$$f_{in} = c_{c1} \frac{\partial^2 w}{\partial t^2} \tag{7}$$

$$f_{vis} = c_{c2} \frac{\partial w}{\partial t} \tag{8}$$

Through dimensional analysis

$$c_{c1} \sim \frac{\rho_c h^2}{h_c}, c_{c2} \sim \frac{\nu_c}{\delta_c}$$

where $\rho_c, \nu_c, h_c, \delta_c$ are the coolant density, the coolant viscosity, the cooling channel thickness, and the thickness of the oscillating boundary layer describing the friction effect, respectively.

The dimensionless variables are defined as

$$W = w/h, \zeta = x/a, \tau = t/\sqrt{\rho h a^4/D}, R_0 = \frac{N_0 a^2}{D}, \mu = \frac{\rho_\infty a}{\rho h}, \lambda = \frac{2q a^3}{D\sqrt{M_\infty^2-1}}$$

$$P_{ch} = \frac{a^4}{Dh} p_{ch}, P_{Gr} = \frac{p_{ch}}{G a}, C_{c1} = \frac{c_{c1}}{\rho h}, C_{c2} = \left(\frac{a^4}{D\rho h}\right)^{1/2} c_{c2}, P_\infty = \frac{a^4}{Dh} p_\infty$$

where $R_0, \mu, \lambda, P_{ch}, P_{Gr}, C_{c1}, C_{c2}$ denote the in-plane load, air/plate mass ratio, freestream dynamic pressure, head-panel pressure, pressure drop ratio, inertial resistance, and viscous resistance, respectively. $P_{ch} = \alpha P_\infty$ is valued near the atmospheric pressure of the incoming flow, where α is coefficient of head-panel pressure. P_{Gr} cannot be less than 1.0. The non-dimensionalised equation of motion is

$$\begin{aligned} & \frac{\partial^2 W}{\partial \tau^2} + \frac{\partial^4 W}{\partial \zeta^4} - 6(1 - \nu^2) \left[\int_0^1 \left(\frac{\partial W}{\partial \zeta}\right)^2 d\zeta \right] \frac{\partial^2 W}{\partial \zeta^2} - R_0 \frac{\partial^2 W}{\partial \zeta^2} \\ & + \lambda \left[\frac{\partial W}{\partial \zeta} + \frac{M_\infty^2 - 2}{M_\infty^2 - 1} \left(\frac{\mu}{\lambda \sqrt{M_\infty^2 - 1}}\right)^{\frac{1}{2}} \frac{\partial W}{\partial \tau} + \frac{\gamma + 1}{4} M_\infty \frac{h}{a} \left(\frac{\partial W}{\partial \zeta}\right)^2 \right] \\ & = \left(\alpha - \frac{\alpha}{P_{Gr}} \zeta - 1\right) P_\infty + C_{c1} \frac{\partial^2 W}{\partial \tau^2} + C_{c2} \frac{\partial W}{\partial \tau} \end{aligned} \tag{9}$$

Equation (9) is solved using Galerkin’s method. The panel deformation can be approximated by a set of sine functions [24,25], which automatically satisfy the simply supported conditions

$$W(\zeta, \tau) = \sum_{n=1}^N a_n(\tau) \sin(n\pi\zeta) \tag{10}$$

The dynamic response of the panel is mainly influenced by the low-order mode. Some research work indicated that the first six modes are sufficient to approximate

the panel deformation [4,14]. Substitute Equation (10) into Equation (9), multiply by $\sin(r\pi\zeta)$ ($r = 1, 2, \dots, N$), and then weighted integrate over the panel length. The result is

$$\begin{aligned} & \frac{(r\pi)^4}{2}a_r + 6(1 - \nu^2) \left[\sum_n \frac{(n\pi)^2}{2} a_n^2 \right] \frac{(r\pi)^2}{2}a_r + R_0 \frac{(r\pi)^2}{2}a_r + \frac{1}{2} \frac{d^2 a_r}{d\tau^2} \\ & + \lambda \left\{ \frac{1}{2} \frac{M_\infty^2 - 2}{M_\infty^2 - 1} \left(\frac{\mu}{\lambda \sqrt{M_\infty^2 - 1}} \right)^{\frac{1}{2}} \frac{da_r}{d\tau} + \sum_n n\pi a_n \delta_{1n} + \frac{\gamma + 1}{4} M_\infty \frac{h}{a} \sum_m \sum_n m\pi a_m n\pi a_n \delta_{2mn} \right\} \quad (11) \\ & = \left[\frac{1 - (-1)^r}{r\pi} (\alpha - 1) + \frac{(-1)^r}{r\pi} \frac{\alpha}{P_{Gr}} \right] P_\infty + \frac{1}{2} C_{c1} \frac{d^2 a_r}{d\tau^2} + \frac{1}{2} C_{c2} \frac{da_r}{d\tau} \quad (r = 1, 2, \dots, N) \end{aligned}$$

where

$$\begin{aligned} \delta_{1n} &= \int_0^1 \cos(n\pi\zeta) \sin(r\pi\zeta) d\zeta \\ \delta_{2mn} &= \int_0^1 \cos(m\pi\zeta) \cos(n\pi\zeta) \sin(r\pi\zeta) d\zeta \end{aligned}$$

Equations (11) are a set of 2-order nonlinear differential equations in time. Important effecting parameters contain $R_0, \lambda, M_\infty, \mu, \alpha, P_{Gr}, C_{c1}, C_{c2}$. Setting $y_r = \frac{da_r}{d\tau}, \frac{dy_r}{d\tau} = \frac{d^2 a_r}{d\tau^2}$, the equations become a set of 1-order differential equations, which are solved by the 4 Runge–Kutta method. In this paper, the material properties and geometrical dimensions are $E = 71.7 \text{ GPa}, \nu = 0.33, a = 1.0 \text{ m}, a/h = 200$. The aircraft flies at an altitude of 30 km. A time step of $\Delta\tau = 0.0001$ and initialization value of $a_1 = 0.0001$ are adopted. All figures are plots at a typical point $\zeta = 0.75$.

Figure 2 shows the close agreement between the stability regions given in [4,14] and the results of the present model where $M_\infty = 5.0, \mu = 0.05, \alpha = 1.0, P_{Gr} = \infty, C_{c1} = 0.0, C_{c2} = 0.0$. Under the coupling effect of freestream and in-plane load, the dynamic characteristics of the panel are complex, including flat and stable, buckled but dynamically stable, Limit Cycle Oscillation (LCO), anharmonic periodic motion, and chaotic motion. In fact, the regions flat and stable and buckled but dynamically stable belong to panel stabilization, whereas the regions LCO and anharmonic periodic motion and chaotic motion belong to panel flutter. The transition process of the motion state of the panel is called bifurcation. Bifurcation is an important nonlinear phenomenon, which means the global behaviors of nonlinear mathematical systems have changed suddenly. Figure 3 compares the peak of LCO from the present model to [4,6,14] when in-plane load $-R_0/\pi^2 = 0, 1, 2, 3$, which shows the close agreement with other reference results. More research on panel flutter with coolant effect is carried out in the following sections.

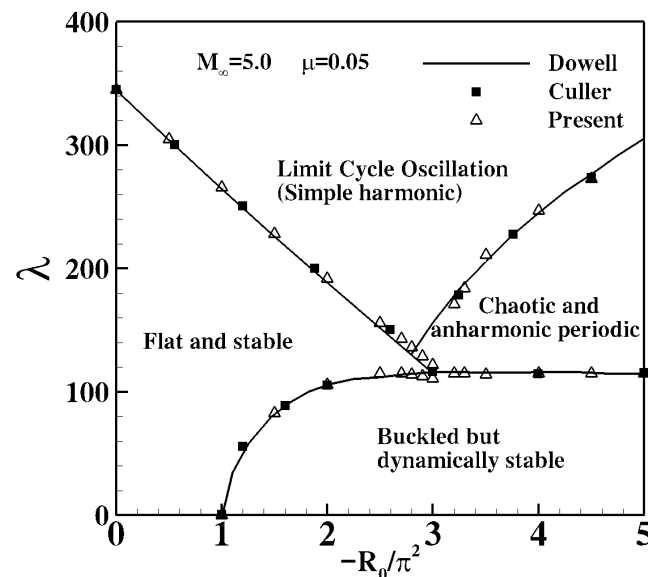


Figure 2. Stability regions.

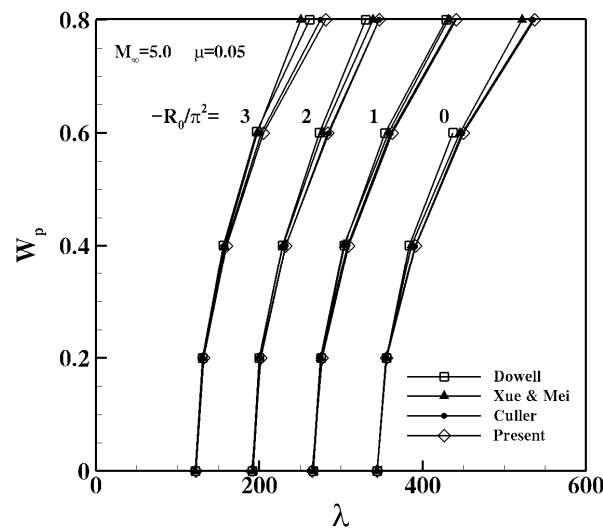


Figure 3. Comparison of the peaks of LCO.

In this section, the dynamic analytical model of panel flutter under the effect of coolant was established. The panel dynamics equations were solved by Galerkin’s method in space domain and the 4th Runge–Kutta method in time domain. The nonlinear modified piston theory was used to predict the unsteady aerodynamic loads. The first six modes were adopted to approximate the panel deformation. Through analysis and derivation, there were eight important effecting parameters: $R_0, \lambda, M_\infty, \mu, \alpha, P_{Gr}, C_{c1}, C_{c2}$, respectively, which affected the characteristics of the panel flutter. In the end, the accuracy of the solution method was verified.

3. Panel Stability

There are five main factors that contribute to the effect of coolant on panel flutter, including the coefficient of head-panel pressure α , the pressure drop ratio P_{Gr} , the coolant injection direction, inertial resistance C_{c1} and viscous resistance C_{c2} . The effect of the pressure drop ratio P_{Gr} on the panel stability, which changes the differential pressure distribution between the upper and lower surfaces of the panel, is discussed first in this section. Figure 4 shows the time history of the panel response at different pressure drop ratios P_{Gr} when λ equals 300.0 and 350.0, respectively. In Figure 4a, the panel is buckled, but the buckling deformation of the panel decreases as the pressure drop ratio increases. When the pressure drop ratio is infinite, the panel is in a flat and stable state. In Figure 4b, the motion morph changes with different pressure drop ratios. It is buckled when P_{Gr} equals 1.0 and 2.0 and LCO when P_{Gr} equals 5.0, 10.0, and ∞ . The amplitude of the LCO increases, and the equilibrium position moves towards 0.

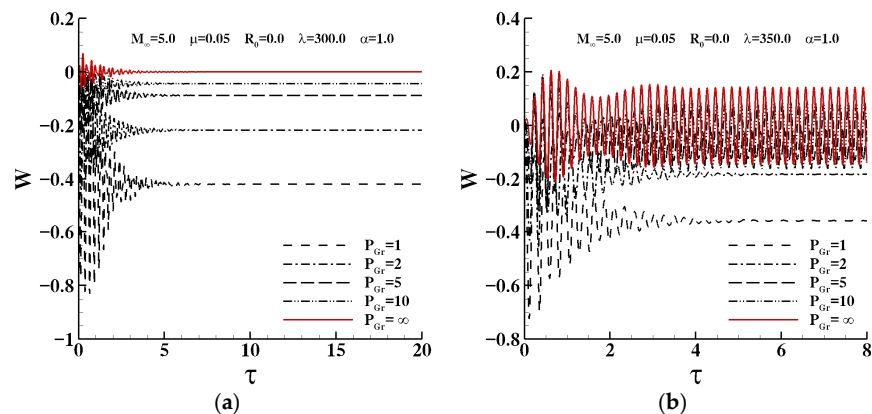


Figure 4. Time history of panel response under different pressure drop ratios: (a) $\lambda = 300$; (b) $\lambda = 350$.

Figure 5 shows the curves of the peak of deformation W_p versus dynamic pressure λ under different pressure drop ratios P_{Gr} . It can be seen that the panel bifurcates from the stable state to LCO, and the critical dynamic pressure λ_{cr} at which bifurcation occurs decreases with increasing P_{Gr} . Some cases are shown. The panel bifurcates from the buckling state to LCO at $\lambda = 420.0$ when $P_{Gr} = 1.0$; moreover, $\lambda = 349.0$ corresponds to $P_{Gr} = 5.0$, and $\lambda = 344.0$ corresponds to $P_{Gr} = \infty$ under which the panel bifurcates from flat and stable to LCO.

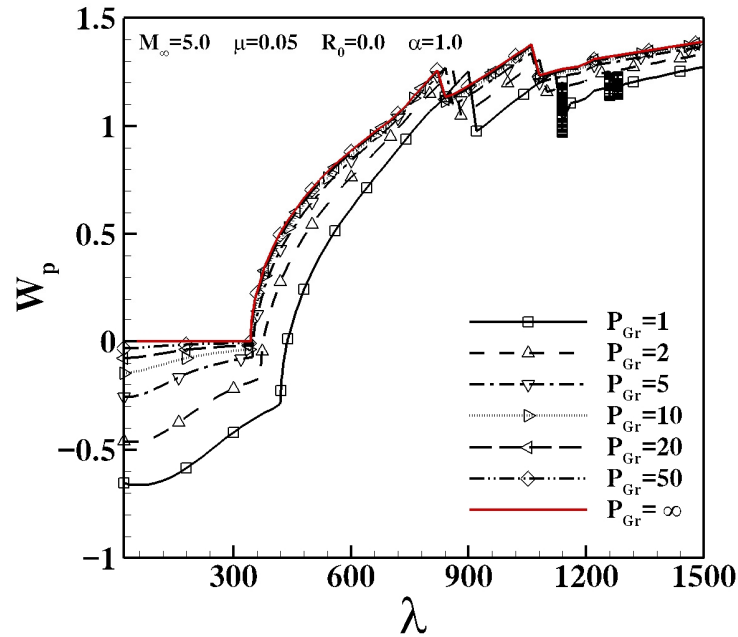


Figure 5. Peak of deformation versus dynamic pressure under different pressure drop ratios.

Figure 6 shows local bifurcation diagrams with several bifurcations of deformation extreme value versus dynamic pressure when $R_0 = -2\pi^2$ and $R_0 = -3.5\pi^2$. In Figure 6a, three bifurcations occur: from the buckling state to the anharmonic periodic motion at $\lambda = 211.7$; from the anharmonic periodic motion to the buckling state at $\lambda = 248.6$; and from the buckling state to the LCO at $\lambda = 263$. In Figure 6b, more than three bifurcations occur, and these are not detailed here.

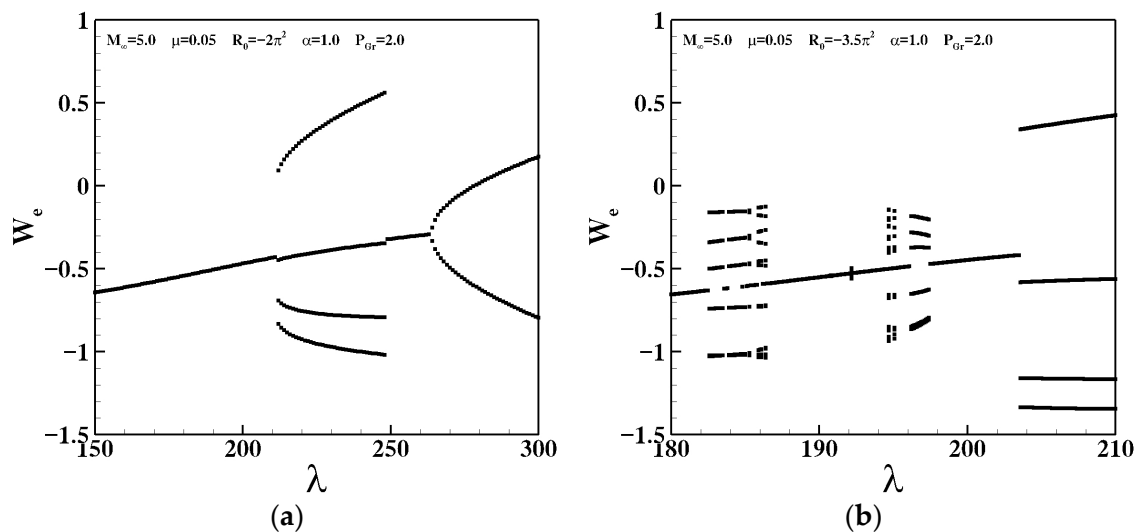


Figure 6. Multiple bifurcations: (a) $R_0 = -2\pi^2$; (b) $R_0 = -3.5\pi^2$.

Set $R_0 = -4\pi^2$. Figure 7 shows the time history and phase diagram of the panel deformation when $\lambda = 150.0$. The panel is in buckling motion and gathers as a point on the phase plane at $P_{Gr} = 2.0$, while the panel performs chaotic motion and the phase diagram is disordered, reflecting strong nonlinearity at $P_{Gr} = 5.0$. Figure 8 shows the results when $\lambda = 350.0$, where anharmonic periodic motion occurs. Bifurcation diagrams with several bifurcations of deformation extreme value versus dynamic pressure are shown in Figure 9. For $P_{Gr} = 2.0$, the first bifurcation of the panel occurs at $\lambda = 186.0$ from the buckling state to the chaotic motion. The second bifurcation occurs at $\lambda = 196.0$ from chaotic motion to anharmonic periodic motion. The third bifurcation occurs at $\lambda = 469.0$ from anharmonic periodic motion to LCO. There are other bifurcations, but they are not mentioned here. They all show the complex and strongly nonlinear nature of the panel dynamic response. For $P_{Gr} = 5.0$, the bifurcation process is similar but with lower critical dynamic pressure than the result for $P_{Gr} = 2.0$. The first three critical dynamic pressures are $\lambda_{cr} = 139.0, 182.0, 395.0$, respectively.

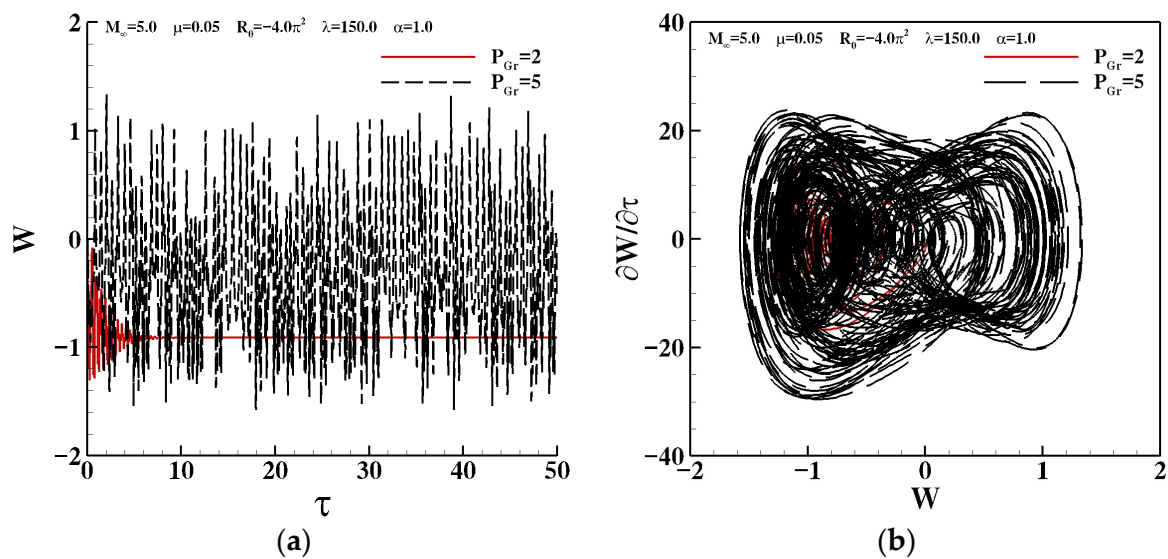


Figure 7. (a) Time history and (b) phase diagram under different pressure drop ratios ($\lambda = 150.0$).

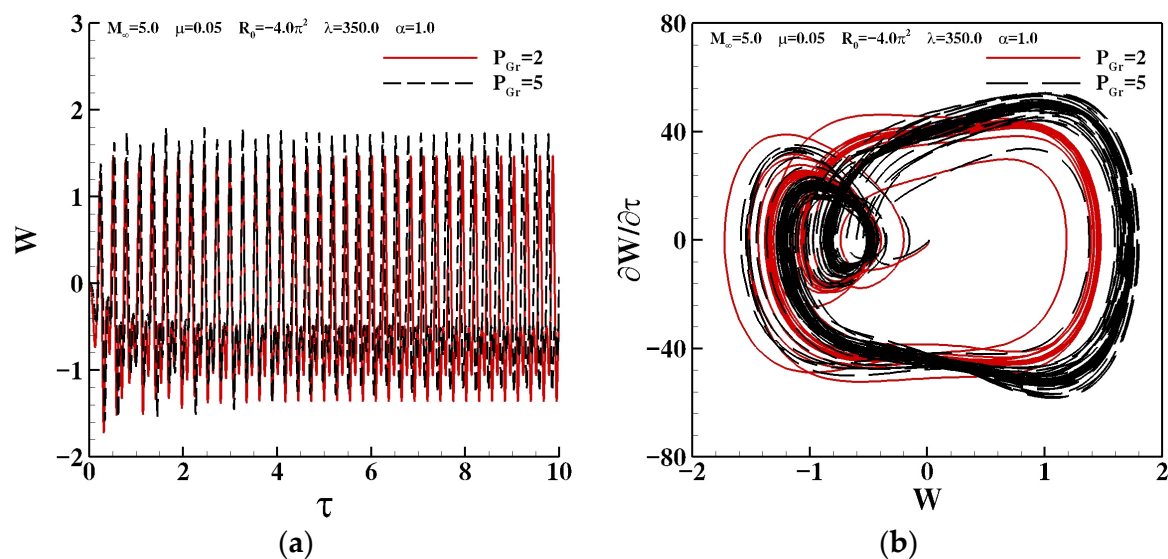


Figure 8. (a) Time history and (b) phase diagram under different pressure drop ratios ($\lambda = 350.0$).

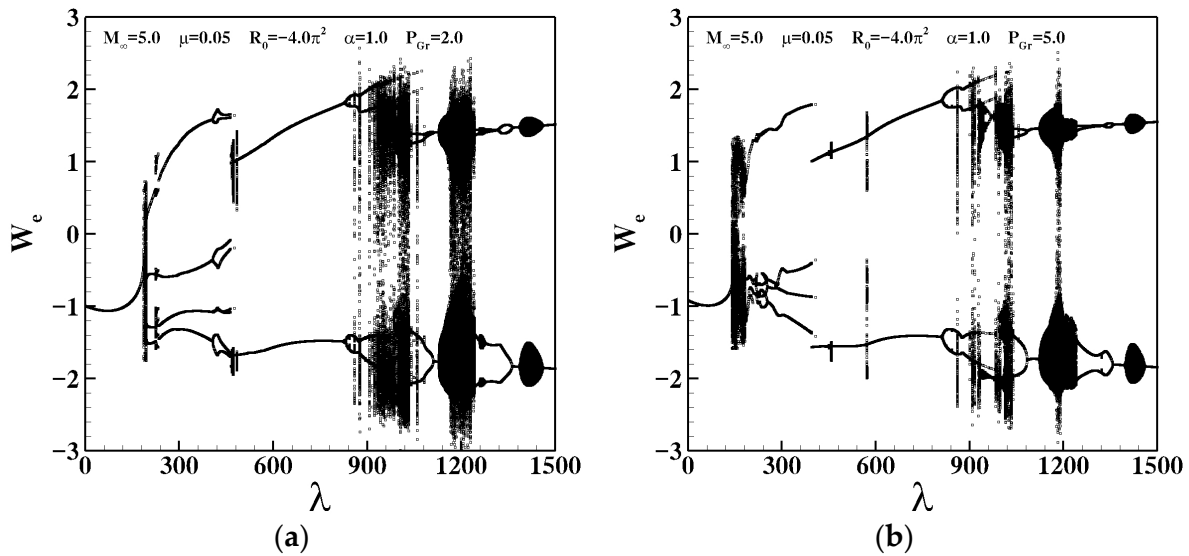


Figure 9. Bifurcation diagrams of deformation extreme: (a) $P_{Gr} = 2.0$; (b) $P_{Gr} = 5.0$.

Based on the above results, the stability regions of the panel with an in-plane load at different pressure drop ratios are shown in Figure 10. These curves divide the $(-R_0/\pi^2) - \lambda$ plane into two regions: the stable and buckled region and the flutter region. The flutter region has complex motion forms, including LCO, anharmonic periodic motion, chaotic motion, etc. The curves indicate a nonfunctional relationship between $-R_0/\pi^2$ and λ . Taking the case with $P_{Gr} = 1.0$ as an example, three critical dynamic pressures exist on the curve when $-R_0/\pi^2 = 2$, which means three bifurcations and at least four panel response forms, which are buckling motion, flutter (anharmonic periodic motion or chaotic motion), buckling motion, and flutter(LCO) in turn. When $-R_0/\pi^2 \in (2.8, 5)$, the panel bifurcates from buckling motion to flutter after which no multiple bifurcations or more complex bifurcation behaviors occur. As the in-plane load increases from 0.0, the critical dynamic pressure of panel flutter decreases as a whole. The stability curves tend to be horizontal with high P_{Gr} and high $-R_0/\pi^2$. A smaller P_{Gr} results in a larger area of stability and buckling region, which means that the panel is more likely to stabilize.

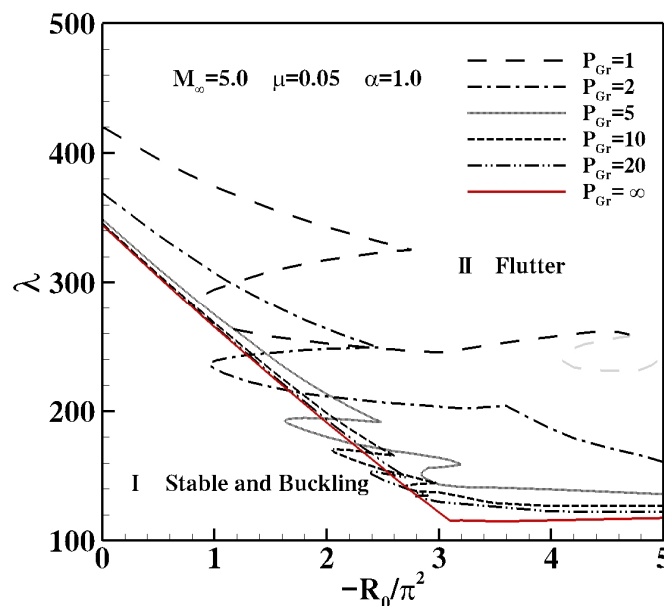


Figure 10. Stability regions under different pressure drop ratios.

The coefficient of head-panel pressure α determines the pressure difference on the surface of the panel, which is another important factor affecting the stability of the panel. Figure 11 plots the peak of deformation versus freestream dynamic pressure λ under different coefficients of head-panel pressure α . It can be seen from Figure 11 that as α increases, the panel bifurcates from buckling motion or stable state to LCO. The buckling deformation and limit cycle amplitude increase gradually and the critical dynamic pressure decreases first and then increases.

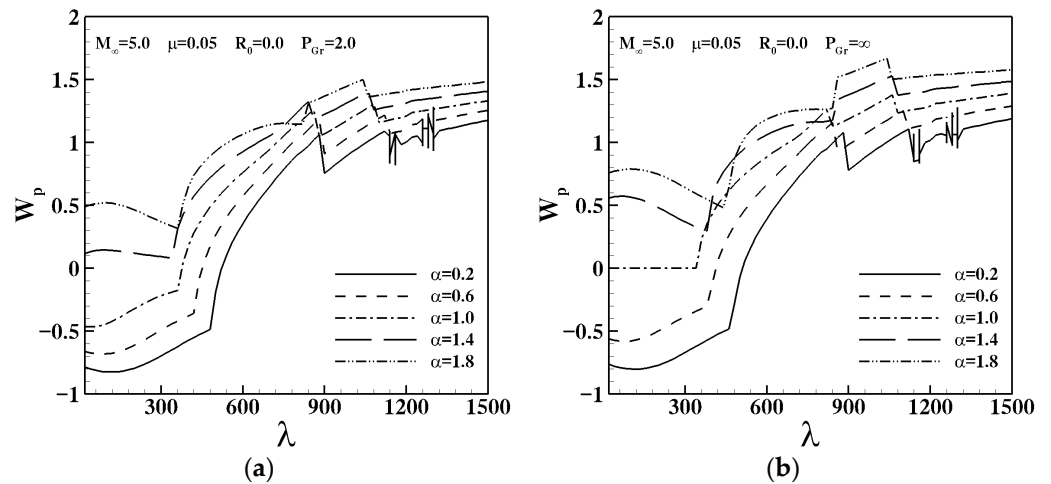


Figure 11. Peak of deformation versus dynamic pressure under different coefficients of head-panel pressure: (a) $P_{Gr} = 2.0$; (b) $P_{Gr} = \infty$.

Figure 12 shows the stability regions of the panel under an in-plane load for different coefficient of head-panel pressure α . With the increase in α , the area of the stable and buckling region decreases first and then increases. The minimum value occurs at $\alpha = 1.4$ when $P_{Gr} = 2.0$, and at $\alpha = 1.0$ when $P_{Gr} = \infty$ among all cases. When $\alpha = 0.2$ and $\alpha = 1.8$, the upper and lower surfaces of the panel have the same static pressure difference in the opposite direction. However, the area of the stable and buckling region is larger when $\alpha = 0.2$ than that when $\alpha = 1.8$. The same result is concluded when $\alpha = 0.4$ and $\alpha = 1.4$. As the in-plane load increases, the critical dynamic pressure of the panel flutter decreases, and meanwhile, three bifurcations and more complex bifurcation behaviors occur.

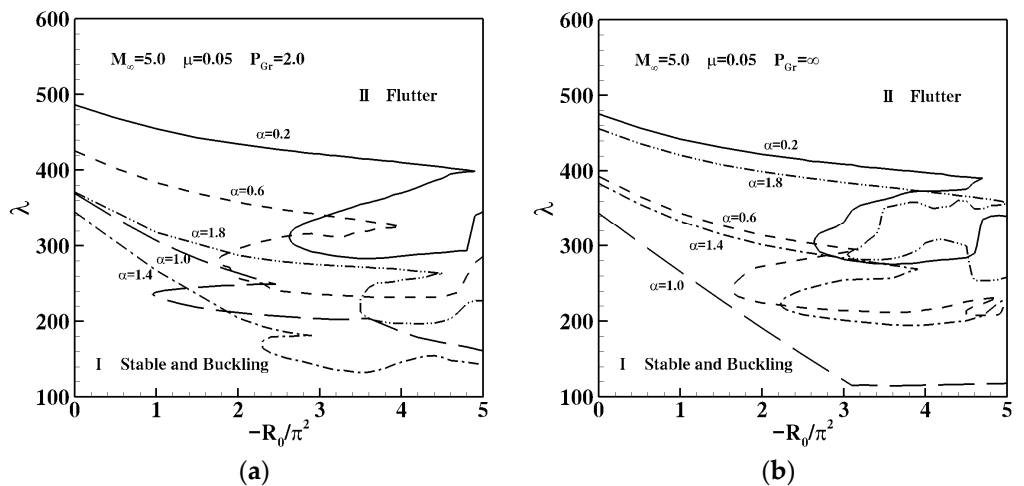


Figure 12. Stability regions under different coefficients of head-panel pressure: (a) $P_{Gr} = 2.0$; (b) $P_{Gr} = \infty$.

Figure 13 shows the relationship between the critical dynamic pressure and the buckling deformation of the panel when the bifurcation occurs. The value α increases from 0.2 to 2.0 along the curves and positive ordinate. The figure mainly reflects two points:

1. Contradiction between the panel deformation and flutter critical dynamic pressure. It is not difficult to see that the panel deformation is increased with the increase in the critical dynamic pressure. Therefore, not only the flight safety but also the strength safety of the material should be considered in the structural design process.
2. The safety envelope and flutter envelope of the panel. The $W \sim \lambda$ plane is divided into three regions by all curve clusters, labeled I, II, and III in Figure 13. No flutter occurs regardless of the P_{Gr} and α values in zone I. Flutter always occurs in zone II. Whether flutter occurs or not depends on the values of (P_{Gr}, α) . The delimitation curves of zones I and III, and zones I and II form the safety envelope and the flutter envelope of the panel, respectively.

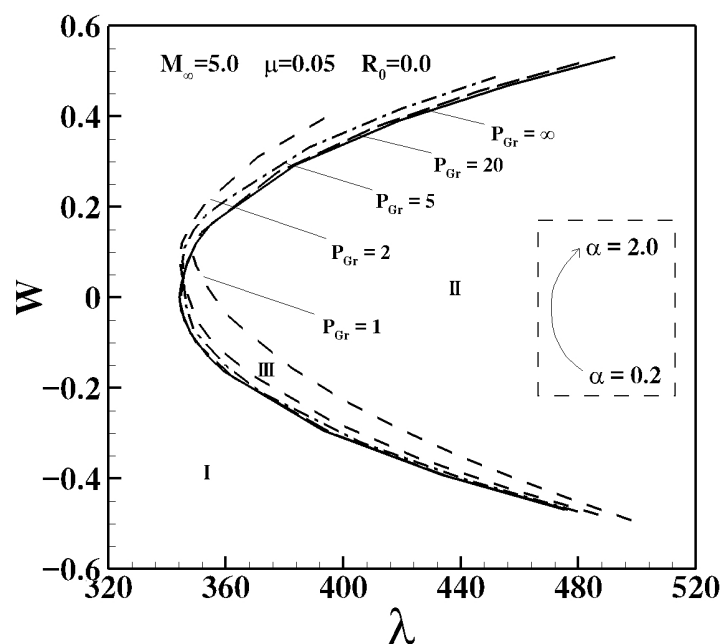


Figure 13. The buckling deformation versus the critical dynamic pressure.

The coolant injection direction is another important factor in the analysis of panel stability. Figure 14 plots the curves of the peak of deformation versus the freestream dynamic pressure under the condition of the forward injection and reverse injection of coolant. The injection direction mainly affects three aspects of the panel response. First, in the buckling state, the buckling deformation under forward injection is smaller than that under the reverse injection when the dynamic pressure is small, while the magnitude relationship changes when the dynamic pressure is large. There is obviously a transition point. With the increase in α , the values of λ corresponding to the transition points are 140, 94, 49.5, and 111.1, respectively. Second, the position at which the bifurcation occurs is also different. The bifurcation occurs first when the coolant is injected reversely when α is equal to 0.6 and 1.0, while opposite results are obtained when α is equal to 1.4 and 1.8. Third, the peak of LCO when the coolant is injected forward is larger than that when the coolant is injected reversely, and the difference between the peaks increases with the increase in α .

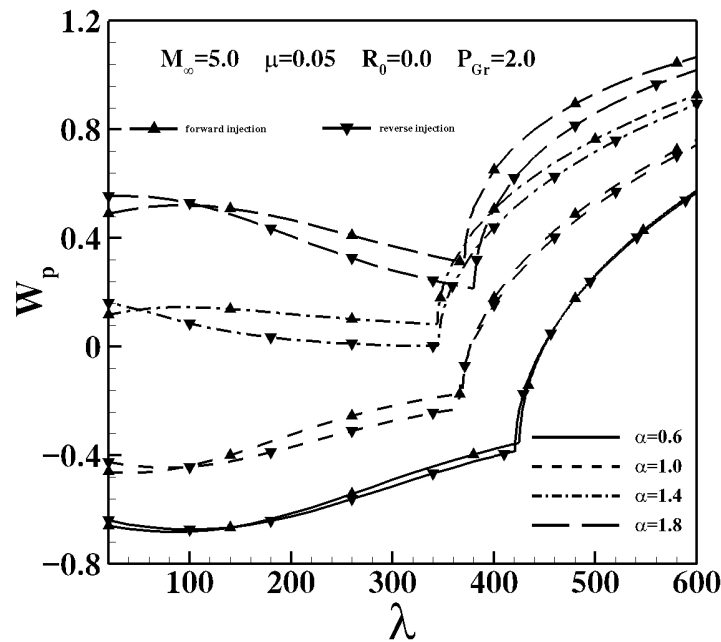


Figure 14. Peak of deformation versus dynamic pressure under different injection directions.

Figure 15 shows the stability regions of the panel under the influence of the coolant injection direction. When $\alpha = 0.6$, the panel with a small in-plane load is more prone to bifurcation using the reverse injection method. The injection method that leads to earlier bifurcation or multiple bifurcations of the panel with a large in-plane load is correspondingly opposite. The effect of the coolant injection direction on the panel stability when $\alpha = 1.8$ is opposite to that when $\alpha = 0.6$. Table 1 shows the critical dynamic pressure of the panel without an in-plane load using different injection methods. The results are close when $\alpha = 1.4$. The result obtained by the reverse injection is smaller than that of the forward injection when $\alpha < 1.4$, and the conclusion is opposite when $\alpha > 1.4$.

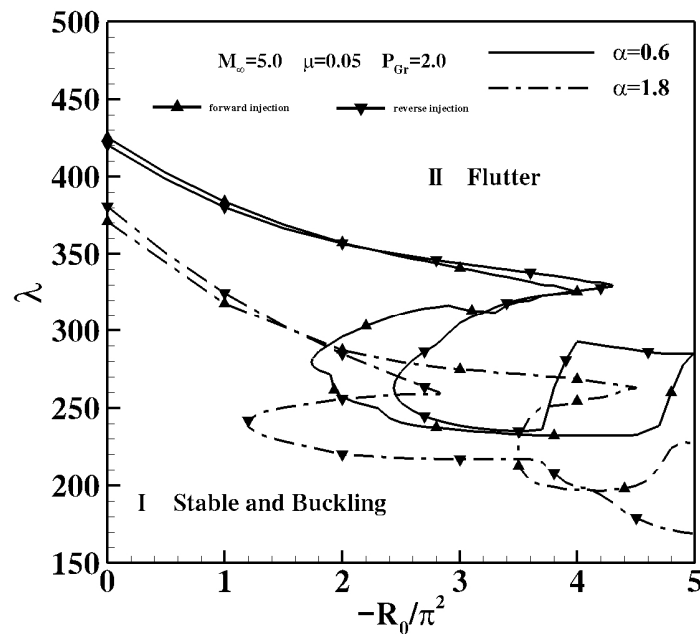


Figure 15. Stability regions under different injection directions.

Table 1. The critical dynamic pressure of the panel without in-plane load under different injection.

α	0.6	1.0	1.4	1.8
λ_{cr} (forward injection)	425.4	369	344.3	370.9
λ_{cr} (reverse injection)	420.5	364.9	345.2	380

Considering the influence of inertial and viscous resistances, Figure 16 shows the convergence process of the buckling response under different inertial and viscous resistances. It indicates that inertial resistance slows down the convergence process, while viscous resistance speeds up the convergence process. However, neither of them change the buckling deformation of the panel. Figure 17 plots the peak of deformation versus the freestream dynamic pressure under different inertial and viscous resistances, showing that the panel bifurcates from the stable state to LCO. In Figure 17a, the critical dynamic pressure of the panel decreases, and meanwhile, the peak of LCO gradually increases as inertial resistance increases, but clear changes appear only at small inertial resistances. Figure 17b shows the influence of viscous resistance, which plays the opposite role to inertial resistance.

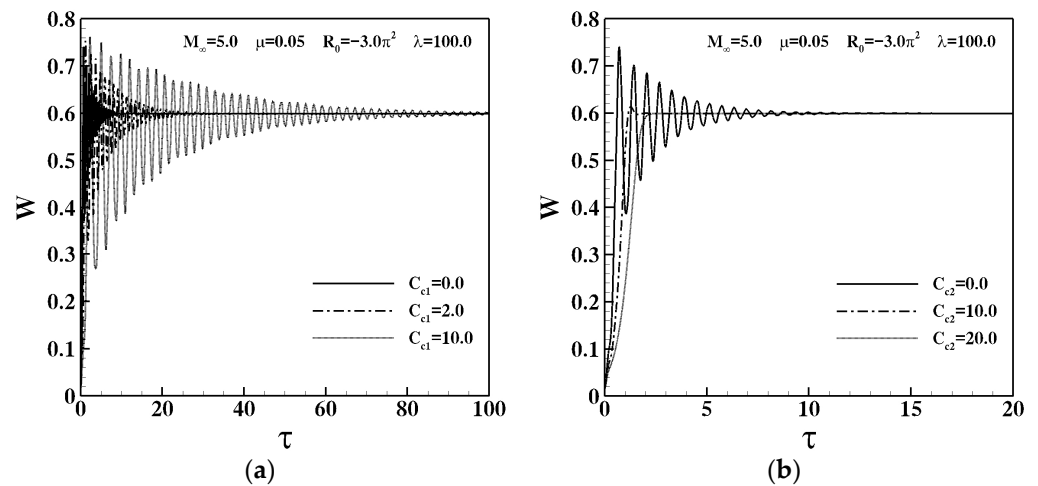


Figure 16. The convergence process of the buckling response under different inertial and viscous resistances: (a) inertial resistances; (b) viscous resistances.

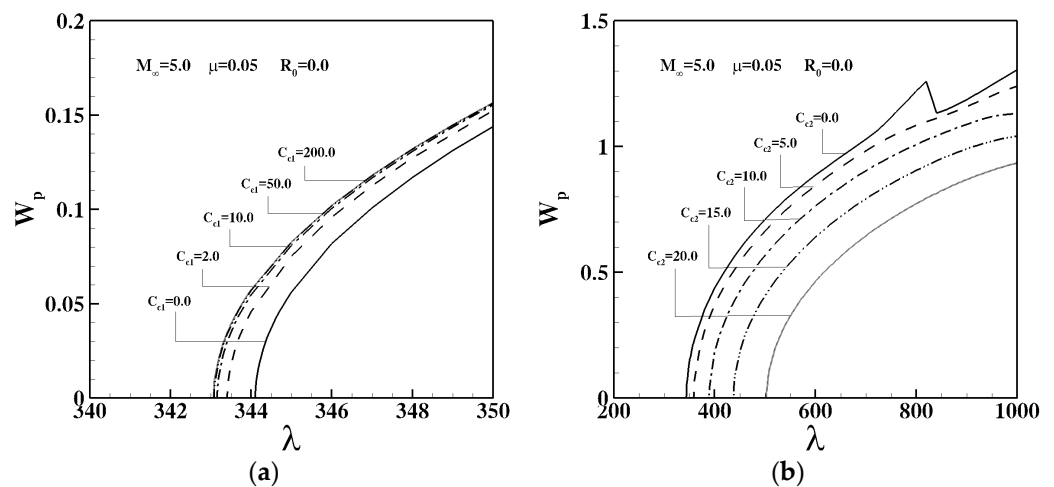


Figure 17. Peak of deformation versus dynamic pressure under different inertial and viscous resistances: (a) inertial resistances; (b) viscous resistances.

Table 2 shows the critical dynamic pressure of the panel under an in-plane load at different inertial resistances. As the in-plane load increases, the critical dynamic pressure first decreases and then tends to be stable. When $-R_0/\pi^2 = 0, 1, 2$, the critical dynamic pressure gradually decreases with increasing inertial resistance. When $-R_0/\pi^2 = 3, 4$, the panel performs multiple bifurcations under the action of large inertial resistances. For instance, the complex multi-bifurcation phenomenon occurs when $\lambda > 119.79$ under the conditions of $-R_0/\pi^2 = 3, C_{c1} = 10.0$. When $-R_0/\pi^2 = 5$, the critical dynamic pressure is almost constant. Figure 18 shows the stability regions of the panel under different viscous resistances. As the in-plane load increases, the critical dynamic pressure first decreases and then tends to be stable. As the viscous resistances increase, the critical dynamic pressure increases gradually for small in-plane loads, and remain almost constant for large in-plane loads.

Table 2. The critical dynamic pressure when bifurcation occurs under different inertial resistances.

$-R_0/\pi^2$	0	1	2	3	4	5
λ_{cr} ($C_{c1} = 0.0$)	344.1	265.41	191.23	121.9	116.45	117.79
λ_{cr} ($C_{c1} = 2.0$)	343.4	264.96	190.99	121.83	116.89	117.79
λ_{cr} ($C_{c1} = 10.0$)	343.14	264.81	190.9	119.79	116.92	117.79
λ_{cr} ($C_{c1} = 50.0$)	343.08	264.75	190.88	114.66	115.17	117.79
λ_{cr} ($C_{c1} = 200.0$)	343.06	264.75	190.87	114.23	110.5	117.79

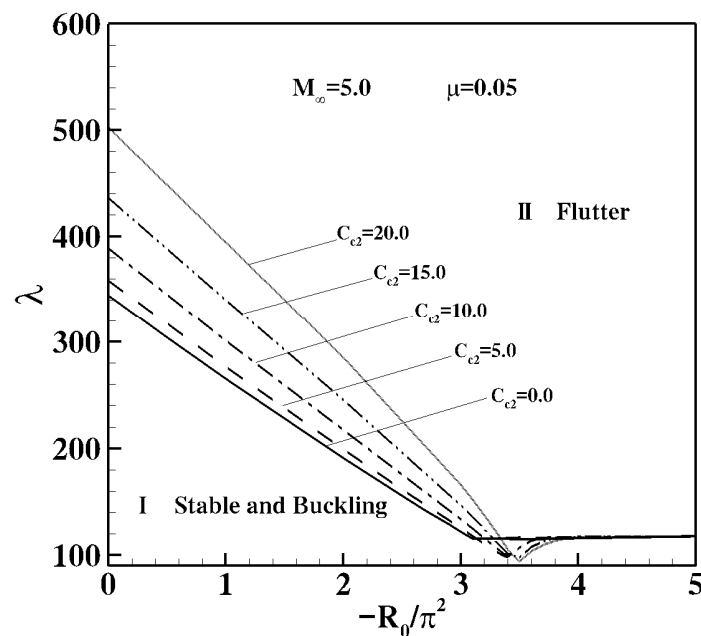


Figure 18. Stability regions under different viscous resistances.

In this section, the stability characteristics of the panel under the action of coolant are presented. The pressure drop ratio with a range of $(1, \infty)$ determines the pressure difference distribution on the surfaces of the panel. The critical dynamic pressure under a low pressure drop ratio is larger than that under a high pressure drop ratio. The coefficient of head-panel pressure determines the magnitude of pressure difference. The critical dynamic pressure is large when the coefficient of head-panel pressure is valued far away

from 1.0. The effect of the coolant injection direction on panel flutter is affected by the pressure drop ratio and the coefficient of head-panel pressure. When the head-panel pressure is low, the critical dynamic pressure under forward injection is larger than that under reverse injection. Inertial resistance slows down the convergence process of the panel response, while viscous resistance speeds up this process. Inertial resistance reduces the critical dynamic pressure but not obviously, while viscous resistance significantly improves the critical dynamic pressure.

4. Flight Stability and Chatter Suppression

The stability of a panel without an in-plane load at the same height but with different Mach numbers is discussed in this subsection. Figure 19 shows the variation in the critical dynamic pressure at the panel bifurcation point with a freestream Mach number for different pressure drop ratios. When P_{Gr} is valued less than 20.0, the critical dynamic pressure gradually increases as the Mach number increases. When $P_{Gr} = 20.0$, the critical dynamic pressure first decreases and then increases, but the variation is very small. When $P_{Gr} = 1.0, 2.0$, the panel bifurcates several times at a high Mach number. For example, when $P_{Gr} = 1.0, M_\infty = 15.0$, the panel bifurcates from buckling motion to anharmonic periodic motion at $\lambda = 330.6$, bifurcates to buckling motion at $\lambda = 283.9$, and bifurcates to LCO at $\lambda = 432.7$, which greatly reduces the safe dynamic pressure of the flight. Figure 19 shows that when $M_\infty < 10.0$, the bifurcation does not occur more than once and the critical dynamic pressure decreases as the pressure drop ratio increases. For $M_\infty = 5.0$, the largest critical dynamic pressure is 420.1 at $P_{Gr} = 1.0$, which is 22.1% higher than the least critical dynamic pressure of 344.0 at $P_{Gr} = \infty$.

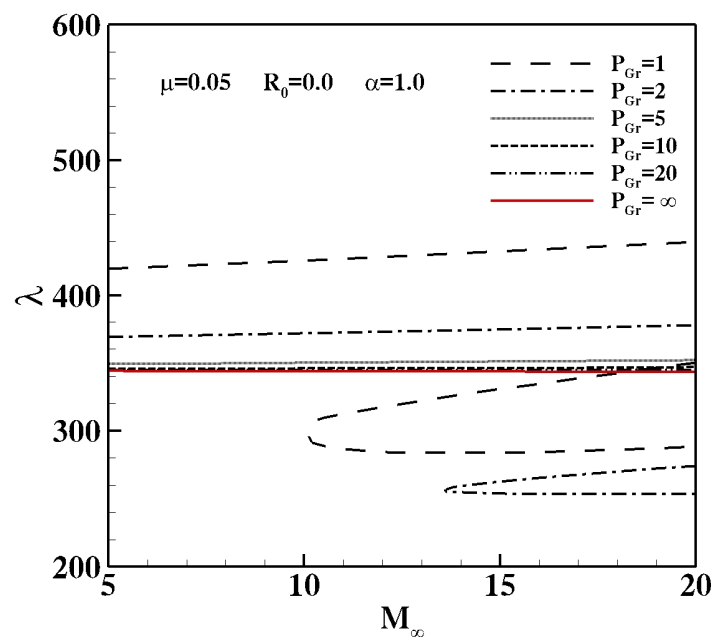


Figure 19. Variation curve of critical dynamic pressure with freestream Mach number for different pressure drop ratios.

Figure 20 shows the variation curves of the critical dynamic pressure of panel flutter with increasing Mach numbers for different coefficients of head-panel pressure. When $\alpha = 0.2, 0.6, 1.0$, the critical dynamic pressure increases with the increase in the Mach number. When $\alpha = 1.4, 1.8$, the critical dynamic pressure decreases with the increase in the Mach number. When $\alpha = 0.6, 1.0$, the panel bifurcates several times at a high Mach number. When $M_\infty < 13.7$, the critical dynamic pressure first decreases and then increases as the value of α increases.

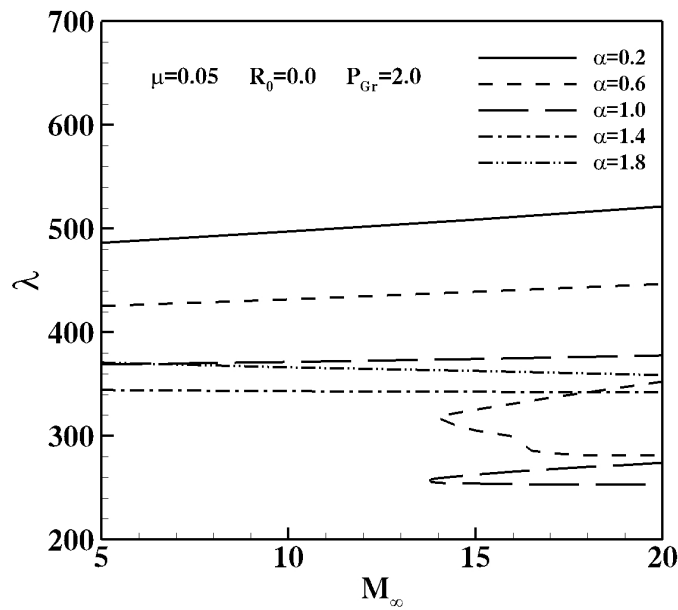


Figure 20. Variation curve of critical dynamic pressure with freestream Mach number for different coefficients of head-panel pressure.

Figures 21 and 22 show the variation curve of the critical dynamic pressure with increasing Mach numbers under inertial resistance and viscous resistance, respectively. It can be seen that all curves in Figures 21 and 22 show a gradually decreasing trend as the Mach number increases. As the inertial resistance increases, the critical dynamic pressure decreases gradually, which has an adverse effect on flight safety, but the effect is very small. For example, when $M_\infty = 5.0$, the critical dynamic pressures are 344.0 at $C_{c1} = 0.0$ and 343.06 at $C_{c1} = 200.0$ with 0.27% difference. When the inertial resistance takes a value above 200.0, the curve is almost horizontal. As the viscous resistance increases, the critical dynamic pressure when panel bifurcation occurs increases significantly, which leads to an obvious suppression effect on the panel flutter. For $M_\infty = 5.0$, the critical dynamic pressures are 344.0 at $C_{c2} = 0.0$ and 502.8 at $C_{c2} = 20.0$ with 50.5% difference.

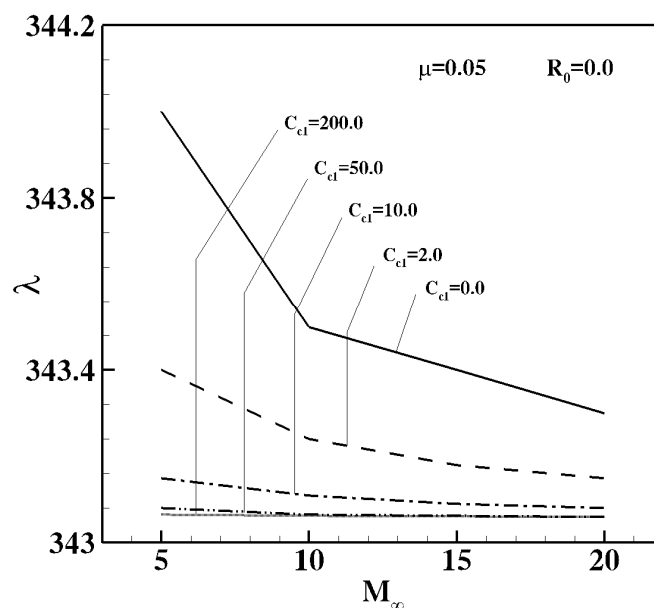


Figure 21. Variation curve of critical dynamic pressure with freestream Mach number for bifurcation of panel under different inertial resistances.

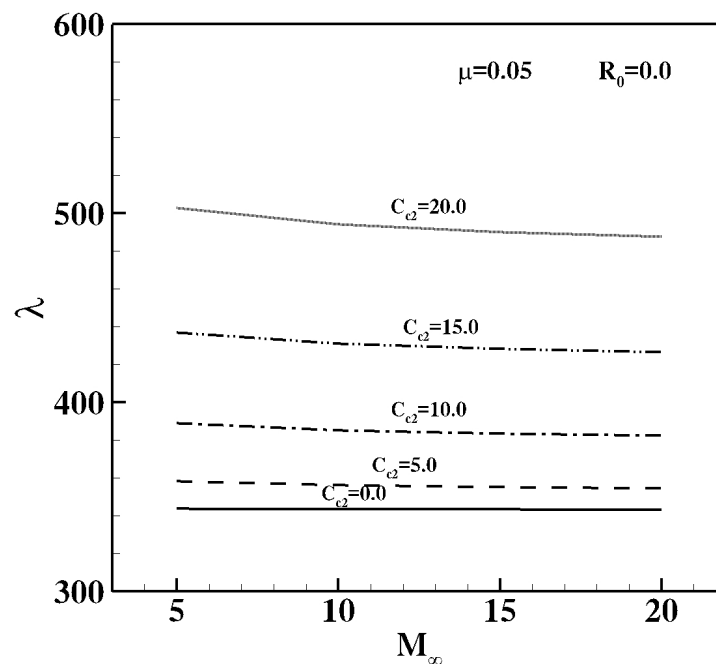


Figure 22. Variation curve of critical dynamic pressure with freestream Mach number for bifurcation of wall plate under different viscous resistances.

The panel shows significantly different stability characteristics under the action of coolant. Therefore, this paper proposes the following solutions to suppress fluttering.

(1) Reduce the pressure drop ratio. However, it should be noted that the problem of the material strength limit caused by large flexural deformation of the structure must be considered under a small pressure drop ratio. If the deformation is required to belong $(-0.2, 0)$ and actual flight dynamic pressure is required to reach 380.0, the pressure drop ratio must be less than 2.0.

(2) Increase or decrease the coefficient of head-panel pressure (away from the value of 1.0). The process brings about a large flexural deformation; therefore, the material strength limit problem also needs to be considered.

(3) Adjust the coolant injection direction. For different head-panel pressures, the coolant injection direction has a different effect on the critical dynamic pressure.

(4) Reduce the inertia resistance and improve the viscous resistance. The inertia resistance slows down the convergence process of the panel response, while the viscous resistance speeds up this process. The inertial resistance reduces the critical dynamic pressure, and the viscous resistance increases the critical dynamic pressure. From the theoretical analysis in Section 2, the inertial resistance is proportional to the coolant concentration, while the viscous resistance is proportional to the coolant viscosity coefficient. Thus, a coolant with a small concentration or a large viscosity coefficient can be selected.

In this section, flight stability of the plate panel is discussed. It can be seen that reducing the pressure drop ratio, and increasing or decreasing the coefficient of head-panel pressure (away from the value of 1.0) can improve the critical dynamic pressure. When the pressure drop ratio is small, the coefficient of head-panel pressure is near 1.0, and the Mach number is high, and the panel is prone to multiple bifurcations occurring. The inertia resistance amplifies the instability of panel flutter, while viscous resistance plays an opposite role. More meaningfully, the flutter suppression strategies are proposed.

5. Discussion and Conclusions

Based on von Karman's large deformation thin plate theory and the Kirchhoff–Love hypothesis, the dynamics model of panel flutter under the action of coolant is established. The accuracy of the analysis model was verified. On this basis, the effects of the head-

panel pressure of coolant, the pressure drop ratio, the coolant injection direction, and the inertial resistance and viscous resistance on panel stability and flight stability were studied, respectively; these are considered to be significant for panel flutter analysis, and the suppression method of panel flutter is proposed. The follow conclusions can be drawn from these results:

(1) The pressure drop ratio determines the pressure difference distribution on the upper and lower surfaces of the panel. A low pressure drop ratio causes multiple bifurcations of the panel with a large in-plane load, and, in general, the critical dynamic pressure when bifurcation occurs under a low pressure drop ratio is larger than that under a high pressure drop ratio. When $M_\infty < 10.0$, the bifurcation occurs no more than one time and the critical dynamic pressure decreases as the pressure drop ratio increases. For $M_\infty = 5.0$, the largest critical dynamic pressure is 420.1 at $P_{Gr} = 1.0$, which is 22.1% higher than the least critical dynamic pressure valued at 344.0 at $P_{Gr} = \infty$. Multiple bifurcations occur at a low Mach number, which greatly reduces the critical dynamic pressure. As the pressure drop ratio decreases, the flexural deformation of the panel when bifurcation occurs increases, so the strength limit of the wall plate material is also considered.

(2) The coefficient of head-panel pressure determines the pressure difference on the upper and lower surfaces of the panel. Values far away from 1.0 can cause a large critical dynamic pressure and avoid multiple bifurcations at high Mach numbers. Moreover, the large panel flexural deformation should be considered.

(3) The coolant injection direction changes the critical dynamic pressure. At low head-panel pressure, the critical dynamic pressure under forward injection is larger than that under reverse injection, while at large head-panel pressure, the result is opposite.

(4) Inertial resistance slows down the convergence process of the panel response, while viscous resistance speeds up this process. Inertial resistance reduces the critical dynamic pressure but not obviously, while viscous resistance significantly improves the critical dynamic pressure. For example, when $M_\infty = 5.0$, the critical dynamic pressures are 344.0 at $C_{c1} = 0.0$ and 343.06 at $C_{c1} = 200.0$ with 0.27% difference, while critical dynamic pressures are 344.0 at $C_{c2} = 0.0$ and 502.8 at $C_{c2} = 20.0$ with 50.5% difference. The critical dynamic pressure gradually decreases as the Mach number increases.

(5) By analyzing the flutter characteristics of the panel under the action of coolant, the suppression strategy of panel flutter is proposed. Reducing the pressure drop ratio, increasing or decreasing the coefficient of head-panel pressure (away from the value of 1.0), and adjusting the coolant injection direction can play a role. When changing these parameters, the problem of the material strength limit caused by large flexural deformation of the structure must be considered. Reducing inertia resistance and improving viscous resistance can also suppress the flutter. Considering the definitions of inertial resistance and viscous resistance, a coolant with a small concentration or large viscosity coefficient can be selected.

Author Contributions: Conceptualization, J.H., G.Z., and G.Y.; formal analysis J.H.; writing—original draft preparation, J.H.; writing—review and editing, W.L. All authors have read and agreed to the published version of the manuscript.

Funding: This research received no external funding.

Institutional Review Board Statement: Not applicable.

Informed Consent Statement: Not applicable.

Data Availability Statement: The data that support the findings of this study are available from the corresponding author, G.Z., upon reasonable request.

Conflicts of Interest: The authors declare no conflict of interest. The funders had no role in the design of the study; in the collection, analyses, or interpretation of data; in the writing of the manuscript; or in the decision to publish the results.

Nomenclature

a	panel length, chordwise
c_{c1}	inertial resistance coefficient
c_{c2}	viscous resistance coefficient
D	bending stiffness of panel
E	elastic modulus
f_c	coolant load
f_{in}	inertial resistance
f_{vis}	viscous resistance
$-G$	pressure gradient of coolant
h	thickness of plate structure
h_c	cooling channel thickness
Ma_∞	Mach number of freestream
N_x	nonlinear membrane load
N_0	in-plane load
p	aerodynamic pressure on panel surface
p_c	coolant pressure
p_{ch}	head-panel pressure
p_∞	pressure of freestream
q	$\rho_\infty U_\infty^2 / 2$, dynamic pressure
t	time
U_∞	velocity of freestream
$w(x)$	panel displacement, transverse
x	chordwise direction, parallel to flat panel surface
z	transverse direction, normal to flat panel surface
δ_c	thickness of the oscillating boundary layer
ν	Poisson's ratio
ν_c	coolant viscosity
ρ	density of plate structure
ρ_c	coolant density
ρ_∞	density of freestream
<i>dimensionless</i>	
a_r	amplitude of rth sine mode
C_{c1}	inertial resistance
C_{c2}	viscous resistance
P_{ch}	head-panel pressure
P_{Gr}	pressure drop ratio
P_∞	pressure of freestream
R_0	in-plane load
W	panel displacement, transverse
α	coefficient of head-panel pressure
λ	dynamic pressure of freestream
μ	air/plate mass ratio
ξ	chordwise direction, parallel to flat panel surface
τ	time
<i>Subscripts</i>	
c	coolant
cr	critical value
e	extreme value
m, n, r	sine mode numbers
p	peak value
∞	freestream

References

1. Lock, M.H.; Fung, Y. *Comparative Experimental and Theoretical Studies of the Flutter of Flat Panel in a Low Supersonic Flow*; Air Force Office of Scientific Research TN 670; United States Air Force, Office of Scientific Research: Arlington, VA, USA, 1961.
2. Dowell, E.H.; Voss, H.M. *Experimental and Theoretical Panel Flutter Studies in the Mach Number Range of 1.0 to 5.0*; AIAA: Reston, VA, USA, 1965; Volume 3, pp. 2292–2304.
3. Ong, C.C. *Flutter of a Heat Shield Panel*; NASA-CR-122855, TM-71-1013-6; Bellcomm INC.: Edmonton, AB, USA, 1971.
4. Dowell, E. Nonlinear oscillations of a fluttering plate. *AIAA J.* **1966**, *4*, 1267–1275. [[CrossRef](#)]
5. Dowell, E. Nonlinear oscillations of a fluttering plate. II. *AIAA J.* **1967**, *5*, 1856–1862. [[CrossRef](#)]
6. Xue, D.Y.; Mei, C. Finite element nonlinear flutter and fatigue life of two-dimensional panels with temperature effects. *J. Aircr.* **1993**, *30*, 993–1000. [[CrossRef](#)]
7. Guo, X.; Mei, C. Application of aeroelastic modes on nonlinear supersonic panel flutter at elevated temperatures. *Comput. Struct.* **2006**, *84*, 1619–1628. [[CrossRef](#)]
8. Song, Z.-G.; Li, F.-M. Active aeroelastic flutter analysis and vibration control of supersonic composite laminated plate. *Compos. Struct.* **2012**, *94*, 702–713. [[CrossRef](#)]
9. Koo, K.-N.; Hwang, W.-S. Effects of hysteretic and aerodynamic damping on supersonic panel flutter of composite plates. *J. Sound Vib.* **2003**, *273*, 569–583. [[CrossRef](#)]
10. Singha, M.K.; Ganapathi, M. A parametric study on supersonic flutter behavior of laminated composite skew flat panels. *Compos. Struct.* **2005**, *69*, 55–63. [[CrossRef](#)]
11. Moosazadeh, H.; Mohammadi, M.M. Time domain aero-thermo-elastic instability of two-dimensional non-linear curved panels with the effect of in-plane load considered. *SN Appl. Sci.* **2020**, *2*, 1705. [[CrossRef](#)]
12. Cheng, G.; Mei, C. Finite Element Modal Formulation for Hypersonic Panel Flutter Analysis with Thermal Effects. *AIAA J.* **2004**, *42*, 687–695. [[CrossRef](#)]
13. Xie, D.; Xu, M.; Dai, H.; Chen, T. New Look at Nonlinear Aerodynamics in Analysis of Hypersonic Panel Flutter. *Math. Probl. Eng.* **2017**, *2017*, 6707092. [[CrossRef](#)]
14. Culler, A.J.; McNamara, J.J. Studies on Fluid-Thermal-Structural Coupling for Aerothermoelasticity in Hypersonic Flow. *AIAA J.* **2010**, *48*, 1721–1738. [[CrossRef](#)]
15. Chen, J.; Han, R.; Liu, D.; Zhang, W. Active Flutter Suppression and Aeroelastic Response of Functionally Graded Multilayer Graphene Nanoplatelet Reinforced Plates with Piezoelectric Patch. *Appl. Sci.* **2022**, *12*, 1244. [[CrossRef](#)]
16. Xing, Y.J.; Sun, B.; Gao, K.; Wang, Z.; Yang, Y. Research Status of Thermal Protection System and Thermal Protection Materials for Aerospace Vehicles. *Aerosp. Mater. Technol.* **2018**, *48*, 9–15.
17. Ellis, D.A.; Pagel, L.L.; Schaeffer, D.M. *Design and Fabrication of a Radiative Actively Cooled Honeycomb Sandwich Structural Panel for Hypersonic Aircraft*; NASA Technical Report; McDonnell Douglas Corp: St Louis, MO, USA, 1978.
18. Castaldi, M.; Leylegian, J.; Chinitz, W.; Modroukas, D. Development of an Effective Endothermic Fuel Platform for Regeneratively-Cooled Hypersonic Vehicles. In Proceedings of the 42nd AIAA/ASME/SAE/ASEE Joint Propulsion Conference & Exhibit, Sacramento, CA, USA, 9–12 July 2006. [[CrossRef](#)]
19. Salas, K.I.; Waas, A. Convective heat transfer in open cell metal foams. *J. Heat Transf. Trans. ASME* **2007**, *129*, 1217–1229. [[CrossRef](#)]
20. Leylegian, J.C.; Chinitz, W.; Benel, G.; Castaldi, M.J. Investigation of Short Contact Time Reactors for Regeneratively Cooled Hypersonic Vehicles. *J. Propuls. Power* **2012**, *28*, 412–422.
21. He, C.; Hu, W.; Mu, L. Optimal control of convection-cooling and numerical implementation. *Comput. Math. Appl.* **2021**, *92*, 48–61. [[CrossRef](#)]
22. Mao, Z.; Xu, Z.; Wang, Q. Shape memory alloy actuator with active cooling device and deflectable winglet application. *Smart Mater. Struct.* **2020**, *29*, 105026. [[CrossRef](#)]
23. Park, S.; Heus, T.; Gentine, P. Role of convective mixing and evaporative cooling in shallow convection. *J. Geophys. Res. Atmos.* **2017**, *122*, 5351–5363. [[CrossRef](#)]
24. Dai, H.H.; Paik, J.K.; Atluri, S.N. The Global Nonlinear Galerkin Method for the Analysis of Elastic Large Deflections of Plates under Combined Loads: A Scalar Homotopy Method for the Direct Solution of Nonlinear Algebraic Equations. *Comput. Mater. Contin.* **2011**, *23*, 69–99.
25. Giunta, G.; Belouettar, S. Higher-Order Hierarchical Models for the Free Vibration Analysis of Thin-Walled Beams. *Math. Probl. Eng.* **2015**, *2015*, 940347. [[CrossRef](#)]

Disclaimer/Publisher's Note: The statements, opinions and data contained in all publications are solely those of the individual author(s) and contributor(s) and not of MDPI and/or the editor(s). MDPI and/or the editor(s) disclaim responsibility for any injury to people or property resulting from any ideas, methods, instructions or products referred to in the content.